

26. F. G. Bordwell *et al.*, *J. Am. Chem. Soc.* **113**, 9790 (1991).
27. F. G. Bordwell, J. A. Harrelson Jr., T.-Y. Lynch, *J. Org. Chem.* **55**, 3337 (1990).
28. In  $[\text{Fe}(\text{III})\text{H}_3\text{1-b}(\text{O})]^{2-}$ , one urea arm of the cavity is disordered. All atoms beyond C4b were split into two fragments and refined with restraints. The refinement led to a 0.48:0.52 ratio in occupancy.
29. M. L. Hopper, E. O. Schlemper, R. K. Murmann, *Acta Crystallogr.* **B32**, 2237 (1982).
30. J. E. Penner-Hahn *et al.*, *J. Am. Chem. Soc.* **108**, 7819 (1986).
31. L. A. Anderson and J. H. Dawson, *Struct. Bonding* **74**, 1 (1991).
32. The O··N distances in  $[\text{Fe}(\text{III})\text{H}_3\text{1b}(\text{O})]^{2-}$  are as follows: O1b··N3b,  $2.732 \pm 0.005$  Å; O1b··N5b,  $2.702 \pm 0.006$  Å; and O1b··N7b,  $2.686 \pm 0.007$  Å.
33. The O··N distances in  $[\text{Fe}(\text{II})\text{H}_3\text{1a}(\text{OH})]^{2-}$  and  $[\text{Fe}(\text{II})\text{H}_3\text{1b}(\text{OH})]^{2-}$  are also  $< 2.900$  Å.
34. The geometry of  $[\text{Fe}(\text{III})\text{H}_3\text{1a}(\text{O})]^{2-}$  was optimized at the UHF/3-21G\* level with Gaussian 98 and assumed  $C_3$  symmetry. The positions of the iron, oxo, and urea nitrogens and hydrogens were relaxed during optimization, whereas those of the other atoms were fixed according to the x-ray structure. The calculated iron-ligand bond distances (Fe1–O1, 1.83; Fe1–N2, 2.27; and Fe1–N<sub>urea</sub>, 2.03 Å) are similar to those found by XRD methods.
35. R. J. Morris and G. S. Girolomi, *Polyhedron* **7**, 2001 (1988).
36. For a discussion on multiple bonding in  $C_3$  symmetric oxometal complexes, see J. M. Mayer, D. L. Thorn, and T. H. Tulip [*J. Am. Chem. Soc.* **107**, 7454 (1985)].
37. P. G. Debrunner, in *Iron Porphyrins Part III*, A. B. P. Lever and H. B. Gray, Eds. (VCH, Weinheim, Germany, 1989), pp. 139–234.
38. L. Que Jr. and A. E. True, in *Progress in Inorganic Chemistry*, S. J. Lippard, Ed. (Wiley, New York, 1990), vol. 38, pp. 97–200.
39. E. Spaltenstein, R. R. Conry, S. C. Critchlow, J. M. Mayer, *J. Am. Chem. Soc.* **111**, 8741 (1989).
40. We thank the NIH (GM50781 to A.S.B. and GM49970 to M.P.H.), ONR-DURIP (9810448 to A. S. B.), E. Münck for use of his Mössbauer spectrometer, and D. Benson, E. Maatta, and R. Schowen for helpful suggestions on the manuscript. Supplementary information available includes the synthetic procedures for all previously unknown compounds and tables and figures for x-ray structural data of  $\text{K}_2[\text{Fe}(\text{II})\text{H}_3\text{1}(\text{OH})] \cdot 4\text{DMA}$  and  $\text{K}_2[\text{Fe}(\text{III})\text{H}_3\text{1}(\text{O})] \cdot 4\text{DMA}$ .

2 May 2000; accepted 20 June 2000

## Folds on Europa: Implications for Crustal Cycling and Accommodation of Extension

Louise M. Prockter<sup>1</sup> and Robert T. Pappalardo<sup>2</sup>

Regional-scale undulations with associated small-scale secondary structures are inferred to be folds on Jupiter's moon Europa. Formation is consistent with stresses from tidal deformation, potentially triggering compressional instability of a region of locally high thermal gradient. Folds may compensate for extension elsewhere on Europa and then relax away over time.

Since 1979 when the two Voyager spacecraft began their survey of the outer solar system's icy satellites, abundant extensional tectonic structures but only tentative examples of compressional structures have been identified (1–3). Suggested explanations for this conundrum include expansion during freezing of ice I, differential cooling of surface and interior, and displacement of high-density ice polymorphs during differentiation of the largest satellites; however, these mechanisms can account for at most a few percent areal expansion (1, 4, 5). Early Galileo spacecraft observations found examples of extreme extension (tens of percent regionally) on Europa and Ganymede (6–8), yet no subduction zones or large-scale compressional features were recognized (9). Thus, the problem of compensating icy satellite extension has been compounded.

The most dramatic and extreme examples of extension on any icy satellite are Europa's dark and gray bands, sites of complete separation of the icy lithosphere above a mobile substrate that has moved up from below to fill the newly created gap (3, 10–12). Morphologic features identified in high-resolution

images suggest that the process is in many ways analogous to terrestrial oceanic rifting and spreading (12), though corresponding subduction zones are absent.

Morphologic evidence for a series of undulations is found in the region of Astypalaea Linea, a smooth, dark band imaged by Galileo at 43 m/pixel (Fig. 1) (13). Astypalaea is inferred to have formed through strike-slip and oblique opening in response to tidally induced stresses (14, 15). The high-resolution Galileo images reveal subtle shading variations crossing Astypalaea Linea almost perpendicular to its trend (Fig. 1A). When a low-pass filter is applied to the image mosaic (16), a series of anticlines (fold crests) and synclines (fold troughs) becomes apparent, with wavelength ~25 km (Fig. 1B). These are most evident within the smooth material of Astypalaea itself, but continue into the ridged plains surrounding the band; thus, the folds postdate the band and the adjacent ridged plains.

Corroborative evidence for the fold interpretation comes from small-scale structures along the inferred anticline and syncline axes. In general, anticline crests are sites of local tensile stress whereas synclines are sites of compressive stress, and corresponding small-scale structures are expected. Three discrete sets of small-scale fractures (troughs) are observed to cut across Astypalaea Linea, many continuing into the surrounding terrain (Figs. 1C and 2). These fractures occur along the crests of the regional-scale anticlines inferred

from shading. The troughs are somewhat anastomosing and less linear than typical European troughs and are unusual in that they occur in fracture sets.

We also find four well-separated sets of small-scale subparallel ridges (Fig. 2). The ridges are short (~2 to 3 km), narrow (~0.5 km), and quite irregular in planform. These small ridges occur within the inferred synclinal lows, trending subparallel to the fold axes (Fig. 1). The ridges are inferred to be compressional structures (folds and/or thrust blocks) formed within regional-scale synclines. They are found within Astypalaea but not within the surrounding ridged plains, perhaps because the band material is more easily deformable or because the structures are more easily identified within the smooth band material.

The identification of folds is significant to the geological history and resurfacing style of Europa, because we can now begin to understand how the satellite's ubiquitous extension (specifically, band formation) is compensated by compression. In the Astypalaea region, we estimate that crest-to-trough fold height is at least ~100 m (in order to be perceived) but no more than ~1 km [which is the greatest topography observed on Europa (17)]. If the folds have a perfect sinusoidal form and volume was conserved during folding, this height range implies a local compressional strain  $\epsilon$  between –0.004% and –0.4%; if the fold limbs are straight in the manner of kink folds, then  $\epsilon$  can be up to –0.9% (18). Some degree of extensional strain has been accommodated by regional-scale folding of the lithosphere, but this relatively small degree of compressional strain is not sufficient to accommodate Europa's abundant extensional deformation.

Several lines of evidence suggest that Europa's shell has been tidally deformed in response to a combination of diurnal and nonsynchronous rotation stresses, which predicts specific surface patterns of compressive and tensile stress that shift on the time scale of each cycle (19–22). The long-period nonsynchronous rotation stress in the Astypalaea area builds by ~80 kPa per degree of rotation (a period of  $>10^4$  years if occurring today) (19, 21). The

<sup>1</sup>Applied Physics Laboratory, Johns Hopkins University, MS 7-366, 11100 Johns Hopkins Road, Laurel, MD 20723, USA. <sup>2</sup>Brown University, Department of Geological Sciences, Box 1846, Providence, RI 02912, USA.

E-mail: louise.prockter@jhuapl.edu; robert\_pappalardo@brown.edu

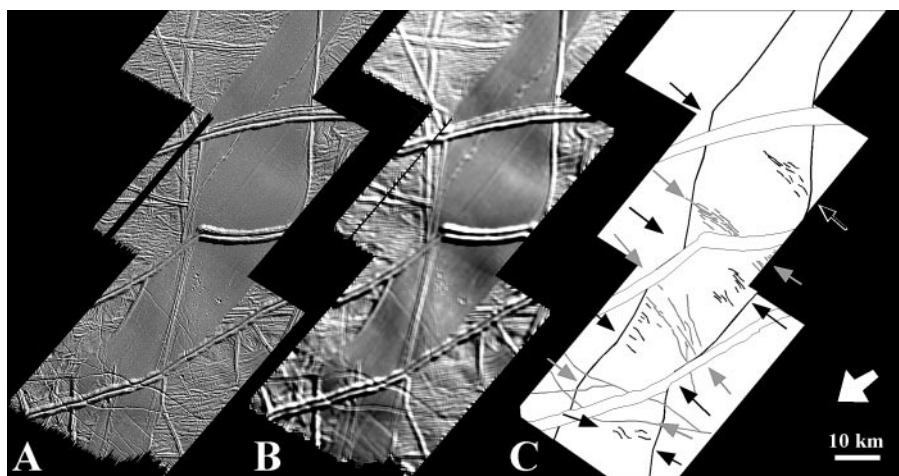


**Fig. 1.** (A) Galileo mosaic of Astypalaea Linea, centered at  $\sim 69^\circ\text{S}$ ,  $198^\circ\text{W}$ . (B) A low-pass filtered image amplifies long-wavelength features, highlighting the anticlines and synclines. (C) Geological map of major features in the imaged area. Fractures mark the anticline crests (gray arrows), and small wrinkle-like ridges (black arrows) are present within synclines (see Fig. 2). North is toward the top; thick white arrow indicates illumination direction. Transmercator projection centered on longitude  $196^\circ\text{W}$ .

short-period diurnal stresses are of lesser magnitude and rotate on the time scale of each 3.55-day orbital cycle (22, 23).

The Astypalaea folds can be used to constrain the character and thickness of the lithosphere at the time of deformation, and the nature of the stresses that likely formed them. The simplest folding model is an elastic layer horizontally compressed over an effectively inviscid substrate (24), either liquid water or warm ice. A nominal Young's modulus  $E \sim 10^9$  Pa (25) implies a layer thickness of  $\sim 1.5$  km and corresponding buckling stress of  $\sim 26$  MPa (26). However, this stress is an order of magnitude more than global stress mechanisms can attain even over many tens of degrees of non-synchronous shell rotation (21, 27). This result discounts simple elastic plate models, including models in which a kilometer-scale elastic shell lies directly above liquid water (22).

Instead, folds may have formed by means of a compressional instability of a frictionally controlled brittle ice lithosphere overlying a warmer ductile asthenosphere in which ice strength decreases with depth (28). If the local thermal gradient is very high ( $\geq 100$  K  $\text{km}^{-1}$ ) and the brittle lithosphere is correspondingly thin ( $\leq 1$  km), lithospheric failure and ductile ice flow can be achieved upon  $\leq 3$  MPa of compressional stress (29). This stress level can accumulate over  $\leq 40^\circ$  of nonsynchronous rotation, during which time local stress orientation would remain broadly consistent with the fold axes. Detailed application of this compressional instability model to Europa for superplastic ice rheology (30) offers promise on the basis of success of its extensional instability counterpart model in

accounting for grooved terrain formation on neighboring Ganymede (31).

The locally high thermal gradient necessary for compressional failure suggests fold formation soon after emplacement of the gray band Astypalaea Linea. The folds have an average orientation of about  $\text{N}50^\circ\text{W}$ , which is  $\sim 20^\circ$  anticlockwise of the current optimum orientation for compressional deformation by nonsynchronous stress. Compressional stress would have been properly oriented when the region rotated through  $\sim 0^\circ$  longitude relative to the satellite's tidal axes. Astypalaea itself is thought to have formed near its current location with respect to tensile tidal stresses (22), but its orientation is also consistent with band formation  $180^\circ$  from its present location (14). This suggests a scenario in which Astypalaea Linea formed near  $20^\circ$  longitude, followed by accumulation of compressional stress and fold formation as the still-warm band rotated through  $\sim 0^\circ$  to  $\sim 340^\circ$  longitude.

Candidate folds are identified in at least two other areas on Europa (32). The gray band Libya Linea was imaged by Galileo at 42 m/pixel (Fig. 3A) (33). A prominent set of anastomosing troughs marks the inferred crest of a single NW-SE-trending anticline that cuts this smooth gray band. The troughs have a complex, branching morphology, and many exhibit terraces. These characteristics are different from those of most European troughs, which are linear and uniform in width. The candidate anticline is flanked by asymmetrical scarps with scalloped, lobate planforms, a morphology characteristic of compressional thrust faults on Earth and other terrestrial planets (34). These scarps are inferred to mark synclines that flank the prominent anticlinal ridge. The inferred syncline-to-syncline separation is  $\sim 12$  km, but the

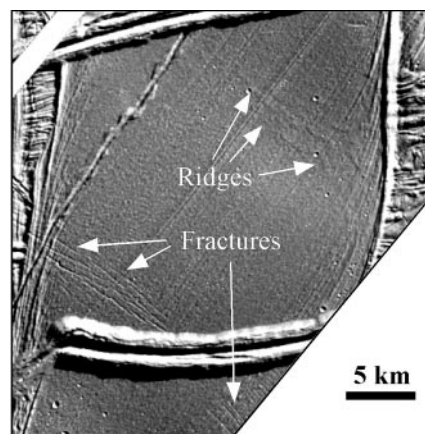


**Fig. 2.** Subsection of Astypalaea Linea showing small-scale ridges in synclines and fractures (troughs) on anticlines, interpreted to be compressional and extensional structures, respectively.

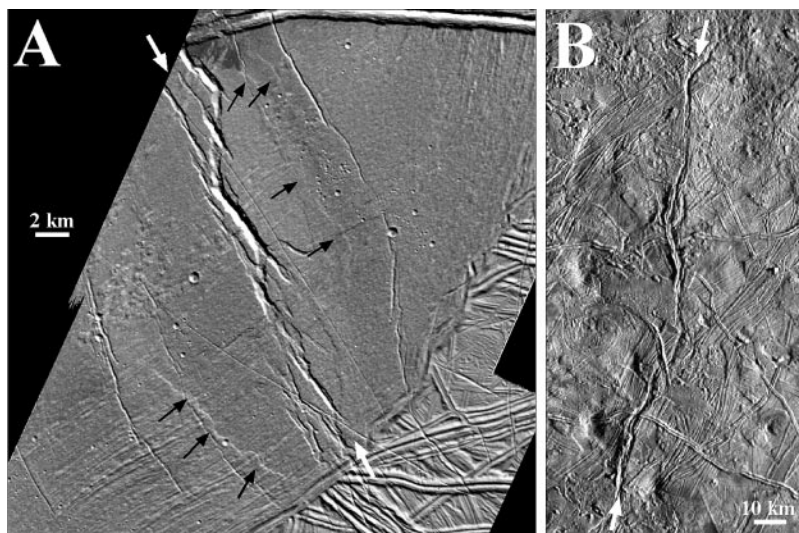


**Fig. 3.** (A) High-resolution Galileo view of Libya Linea. White arrows indicate anastomosing fractures that mark the inferred anticlinal crest, and black arrows indicate inferred synclinal thrust blocks. (B) Regional Galileo mosaic within the Manannán region. White arrows indicate distinctive sinuous fractures with associated subtle brightness variations, inferred as the surface expressions of anticlines.

imaged area is too small to determine whether the anticline and flanking synclinal depressions are isolated or part of a fold set. On the basis of subtle shading variations, anastomosing fractures imaged at 220 m/pixel in the Manannán region may mark the anticlinal crests of regional-scale folds [(35); Web fig. 1 (36)] (one of the fractures is shown in Fig. 3B). The spacing between these structures varies from ~16 to 46 km. Both Libya Linea (a gray band) and the Manannán region (where there is abundant chaotic terrain) may have been areas of high heat flow and thin brittle lithosphere at the time of fold formation.

Our results shed light on the ways in which Europa may hide its compression. The Astypalaea folds are identifiable because they were imaged at a relatively large solar incidence angle (13). Similar subtle undulations may be widespread on Europa but would be difficult to identify because of Galileo's limited imaging coverage. Moreover, Europa's regional-scale topography is expected to relax away through lateral flow of subsurface material if the shallow subsurface is warm (37). Specifically, ~25 km topography is expected to relax in  $\leq 10^5$  years (38). Such a rapid time scale suggests that the observed folds may have formed with greater amplitude (and therefore strain) and may be partially relaxed today. Small-scale fracture and ridge topography should remain, but would be difficult to recognize among the complex maze

of overlapping surface features that compose Europa's ridged plains. As regional stresses shift due to nonsynchronous rotation, small-scale fractures that originated along anticlinal crests may eventually be exploited by tensile tidal stress, opening into ridges or bands.

In summary, we suggest a possible scenario by which Europa's surface is cycled (Fig. 4): (i) new mobile material upwells and cools along extended band axes; (ii) tidally induced compressive stress causes folding in regions of relatively high heat flow and thin lithosphere, such as bands, accommodating extension; and (iii) regional-scale fold topography relaxes vertically, resulting in localized thickening and the corresponding cycling of lithospheric material back into the warm ice interior, leaving only small-scale structures behind. It appears that Europa's ductile ice asthenosphere (39) is key in both creation and loss of fold topography.

References and Notes

1. S. W. Squyres and S. K. Croft, in *Satellites*, J. A. Burns and M. S. Matthews, Eds. (Univ. of Arizona Press, Tucson, AZ, 1986), pp. 293–341.
2. P. M. Schenk and J. M. Moore, in *Solar System Ices*, B. Schmitt et al., Eds. (Kluwer Academic, Norwell, MA, 1998), pp. 551–578.
3. P. M. Schenk and W. B. McKinnon, *Icarus* **79**, 75 (1989).
4. S. Mueller and W. B. McKinnon, *Icarus* **76**, 437 (1988).
5. J. Hillier and S. W. Squyres, *J. Geophys. Res.* **96**, 15665 (1991).
6. R. Sullivan et al., *Lunar Planet. Sci. Conf.* **27**, 1343 (1997).
7. R. T. Pappalardo and G. C. Collins, *Lunar Planet. Sci. Conf.* **30** (abstract 1773), (1999).
8. These Galileo-based estimates are for relatively small regions (<10,000 km<sup>2</sup>) of each satellite's surface. Full accounting of the global extensional strain for Europa and Ganymede has not yet been performed and is made difficult by the limited areal coverage of the regional and high-resolution Galileo image data.
9. On the basis of Voyager images, Europa's bright band Ageron Linea was suggested to be a compressional structure (3), but analysis of Galileo images indicates a strike-slip origin [L. M. Prockter, R. T. Pappalardo, J. W. Head, *J. Geophys. Res.* **105**, 9483 (2000)]. Europa's cycloidal features were also considered possibly compressional (3), but these are now recognized as ridges and fractures with no significant compressional component [G. V. Hoppa et al., *Science* **285**, 1899 (1999)]. Some small-scale ridges and troughs on Europa (wavelength ~500 m) might be folds [J. W. Head et al., *Lunar Planet. Sci. Conf.* **29** (abstract 1412) (1998)], but the identification is tentative.
10. R. Sullivan et al., *Nature* **391**, 371 (1998).
11. R. T. Pappalardo and R. J. Sullivan, *Icarus* **123**, 557 (1996).
12. L. M. Prockter et al., *Lunar Planet. Sci. Conf.* **30** (abstract 1900) (1999).
13. High-resolution images of Astypalaea Linea (observation 17ESSTRSLP01) were obtained during Galileo's 17th orbit, with a solar incidence angle of ~77° (measured from the surface normal), an emission angle of ~45°, and a phase angle of ~32°. Figure 1 is a mosaic of Galileo images s0466670100, s0466670113, and s0466670126.
14. B. R. Tufts et al., *Icarus* **141**, 53 (1999).
15. G. Hoppa et al., *Icarus* **141**, 287 (1999).
16. A 21 × 41 boxcar filter was applied, using the ISIS image software package developed by the U.S. Geological Survey, Flagstaff, AZ.
17. R. T. Pappalardo et al., *J. Geophys. Res.* **104**, 24015 (1999).
18. Strain  $\epsilon \equiv (L_f - L_o)/L_o$ , where  $L_o$  is initial length and  $L_f$  is final length. If a fold of wavelength  $\lambda$  has a sinusoidal form with amplitude  $A$  (crest-to-trough height  $y = 2A$ ),

then  $L_o \approx \lambda + \pi^2 A^2/\lambda$  [H. Ramberg, *Gravity, Deformation and the Earth's Crust* (Academic Press, New York, ed. 2, 1981), p. 169]. For a kink fold with straight limbs that slope at an angle  $\delta$  from horizontal,  $L_o = \lambda + 2(y \csc \delta - y \cot \delta)$ . The Astypalaea folds trend approximately orthogonal to the illumination direction, so if they are kink folds, the solar incidence angle of the images (13) implies that their limbs cannot dip more steeply than 13°, because the fold limbs are not in shadow.

19. P. Helfenstein and E. M. Parmentier, *Icarus* **61**, 175 (1985).
20. A. S. McEwen, *Nature* **321**, 49 (1986).
21. A. C. Leith and W. B. McKinnon, *Icarus* **120**, 387 (1996).
22. R. Greenberg et al., *Icarus* **135**, 64 (1998).
23. G. V. Hoppa et al., *Science* **285**, 1899 (1999).
24. M. A. Biot, *J. Franklin Inst.* **267**, 211 (1959); *J. Franklin Inst.* **270**, 190 (1960); *Geol. Soc. Am. Bull.* **72**, 1595 (1961); S. C. Solomon and J. W. Head, *J. Geophys. Res.* **89**, 6885 (1984).
25. Young's modulus for laboratory samples of polycrystalline ice is  $\sim 9 \times 10^9$  Pa [M. Mellor, in *Physics and Mechanics of Ice*, P. Tryde, Ed. (Springer-Verlag, New York, 1980), pp. 217–245], but cracks and porosity would tend to decrease the Young's modulus of a real ice lithosphere.
26. For elastic plate buckling (24), the effective thickness  $h_e$  and dominant folding wavelength  $\lambda$  are related through Young's modulus  $E$ , Poisson's ratio  $\nu$ , substratum density  $\rho$ , and gravitational acceleration  $g$  as  $h_e = (\rho g/B)^{0.33} (\lambda/2\pi)^{1.33}$ , where  $B = E/12(1 - \nu^2)$ . We adopt  $\nu = 0.33$ ,  $\rho = 920$  kg m<sup>-3</sup>, and  $g = 1.31$  m s<sup>-2</sup> for Europa (17, 21). The corresponding compressive stress to achieve elastic buckling at this wavelength is  $\sigma_b = 2B^{0.33} (\rho g \lambda/2\pi)^{0.67}$ .
27. Reduction of Young's modulus  $E$  below its nominal value does not aid the situation, because nonsynchronous rotation stresses are also proportional to  $E$  (19, 21, 22).
28. D. L. Herrick and D. J. Stevenson, *Icarus* **85**, 191 (1990).
29. Based on analysis of the strength envelope in figure 10 of (17), as modified for lithospheric failure in compression.
30. D. L. Goldsby and D. L. Kohlstedt, *Scr. Mater.* **37**, 1399 (1997).
31. A. J. Dombard and W. B. McKinnon, in preparation.
32. Since the submission of this manuscript, it has come to our attention that regional-scale undulations with a wavelength of ~25 km have also been identified in the leading hemisphere of Europa [P. Figueredo and R. Greeley, *J. Geophys. Res.*, in press].
33. High-resolution images of Libya Linea (observation 17ESLIBLIN01) were obtained during Galileo's 17th orbit, centered at 52°S, 178°W, with an incidence angle of ~59°, an emission angle of ~20°, and a phase angle of ~40°.
34. R. T. Pappalardo and R. Greeley, *J. Geophys. Res.* **100**, 18985 (1995).
35. Images in the Manannán region (observation 11ESREGMAP01; ~10°N–10°S, ~230°–245°W) were obtained during Galileo's 11th orbit, with an incidence angle of ~75° to 82°, an emission angle of ~16° to 33°, and a phase angle of ~58°.
36. Supplementary material is available at [www.sciencemag.org/feature/data/1050255.shl](http://www.sciencemag.org/feature/data/1050255.shl)
37. P. J. Thomas and G. Schubert, *J. Geophys. Res.* **91**, 453 (1986).
38. We apply equation (4) of (37) to model a cold ice layer of viscosity 10<sup>21</sup> Pa·s above warm ice (assumed inviscid) at 1.5 km depth (17).
39. R. T. Pappalardo, J. W. Head, and the Galileo Imaging Team, *Lunar Planet. Sci. Conf.* **30** (abstract 1967) (1999).
40. We thank C. Phillips for mosaic construction, R. Tufts for image targeting, H. Breneman for execution of the E17 sequence, J. Klemaszewski for image playback coordination, and J. Head, G. Collins, J. Moore, and C. Paranicas for valuable discussions. L.M.P. is funded by an Applied Physics Laboratory Postdoctoral Fellowship; R.T.P. acknowledges support from NASA's Jupiter System Data Analysis Program.

9 March 2000; accepted 20 June 2000

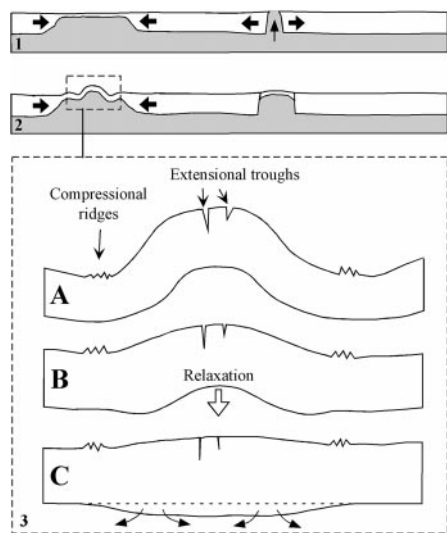


**Fig. 4.** A possible scenario for cycling Europa's lithosphere: (1) Bands form as lithospheric material (white) is pulled apart and mobile material (gray) wells up into newly created gaps; tidally induced compressive stress accumulates in new bands and elsewhere on the surface. (2) Extensional strain is ultimately accommodated by formation of folds in regions of relatively warm and thin lithosphere, such as bands. (3) Regional-scale fold topography relaxes (A and B), and the warm ductile base of the lithosphere is able to flow back into the interior (C); only small-scale surface structures remain, and these structures may later be exploited to form ridges and bands.